Wind and Structures, *Vol. 20, No. 5 (2015) 643-660*
DOI: http://dx.doi.org/10.12989/was.2015.20.5.643

Mechanism on suppression in vortex-induced vibration of bridge deck with long projecting slab with countermeasures

Zhiyong Zhou[a], Ting Yang, Quanshun Ding[*] and Yaojun Ge[b]

State Key Laboratory for Disaster Reduction in Civil Engineering,
Transport Industry Key Laboratory for Wind Resistance Technique in Bridge Engineering, Tongji University, Shanghai 200092, China

(Received March 6, 2014, Revised March 13, 2015, Accepted March 19, 2015)

Abstract. The wind tunnel test of large-scale sectional model and computational fluid dynamics (CFD) are employed for the purpose of studying the aerodynamic appendices and mechanism on suppression for the vortex-induced vibration (VIV). This paper takes the HongKong-Zhuhai-Macao Bridge as an example to conduct the wind tunnel test of large-scale sectional model. The results of wind tunnel test show that it is the crash barrier that induces the vertical VIV. CFD numerical simulation results show that the distance between the curb and crash barrier is not long enough to accelerate the flow velocity between them, resulting in an approximate stagnation region forming behind those two, where the continuous vortex-shedding occurs, giving rise to the vertical VIV in the end. According to the above, 3 types of wind fairing (trapezoidal, airfoil and smaller airfoil) are proposed to accelerate the flow velocity between the crash barrier and curb in order to avoid the continuous vortex-shedding. Both of the CFD numerical simulation and the velocity field measurement show that the flow velocity of all the measuring points in case of the section with airfoil wind fairing, can be increased greatly compared to the results of original section, and the energy is reduced considerably at the natural frequency, indicating that the wind fairing do accelerate the flow velocity behind the crash barrier. Wind tunnel tests in case of the sections with three different countermeasures mentioned above are conducted and the results compared with the original section show that all the three different countermeasures can be used to control VIV to varying degrees.

Keywords: bridge deck with long projecting slab; vortex-induced vibration; wind fairing; CFD; large-scale sectional model test; mechanism

1. Introduction

Flow around bluff bodies typically results in separation of boundary layer and rolls up of separation shear layer, which will finally form alternating vortex shedding flow phenomena. The fluctuating pressures around bluff bodies will cause nonlinear fluid-structure interactions, known as VIV.

Comprehensive fundamental studies on VIV have been performed (Bearman 1984, Gabbai and

*Corresponding author, Associate professor, E-mail: qsding@tongji.edu.cn
[a] Professor, E-mail: z.zhou@tongji.edu.cn
[b] Professor, E-mail: yaojunge@tongji.edu.cn

http://www.techno-press.org/?journal=was&subpage=8 ISSN: 1226-6116 (Print), 1598-6225 (Online)

Benaroya 2005, Sarpkaya 2004, Williamson and Govardhan 2004). In recent decades, most studies have primarily focused on a bluff body with a simple configuration, for example, circular cylinders and rectangular prisms (Sanchez-Sanz *et al*. 2009, Prasanth *et al.* 2008, Wang *et al.* 2005). However, little is understood on the VIV mechanism and flow patterns for more complicated configurations, for example, a stream-lined box girder, which is extensively used in modern long-span cable-supported bridges.

Recent projects of long-span bridges strengthen the need to investigate the low reduced velocity range because of the increase in the structure dimension. Recent full-scale observations also suggest that many bridge decks are prone to VIV in a relatively low wind velocity range for winds approaching almost perpendicular to the bridge axis with low turbulence intensity (Li *et al.* 2011). Although VIV response is not as dangerous as flutter or galloping, it must be carefully taken into account since it can interfere with other aeroelastic effects and can influence the fruition and the fatigue life of the structure. Therefore, the evaluation and control of VIV has been a more and more important subject among the wind-resistance research on bridge aerodynamic appendices to control and reduce vortex shedding. The basic principle of VIV suppression by using countermeasures is to change the aerodynamic configuration of bridge deck section by which to change the air flow and separation around the body surface, destroy the formation or its drift of the vortex, thus suppress VIV in integral effect.

Though different countermeasures according to specific box girder can be found to control VIV of it efficiently, but the mechanism of VIV suppression cannot be explained quantitatively and precisely yet, due to the limits in understanding of fluid-solid coupling vibration (Li 2014). At present, a number of beneficial attempts at the research on VIV mechanism have been made by many scholars based on the wind tunnel test or CFD numerical simulation. Diana (2006, 2013) performed experimental tests on the multi-box deck shape of the Messina Strait bridge investigating vortex shedding phenomena. The experimental tests, focused on low reduced velocities, highlight the typical non-linear pattern of the vortex shedding. The porous screens between the railway box and the road boxes were adopted to avoid VIVs also for lower values of structural damping. In order to acquire better understanding of the VIV mechanism, some mathematical model have been developed to reproduce the vortex shedding forces (Diana 2006, 2008, Wu 2013 and Antonino 2011). Nagao (Nagao 1997) studied the effects of handrail on the response of VIV based on smoking agent and pressure measurement in macroscopic perspectives. The results showed that some handrails would give rise to VIV and almost all the handrails would increase the amplitude of vertical VIV. Ricciardelli (2002) performed some experiments of VIVs of Sunshine Skyway deck in the smooth flow field and analyzed these phenomenon from the surface pressure distribution, three-component force, structural response and velocity field of wakes. EI-Gammal (2007) measured the surface pressure around model bridge and the velocity distribution of wake when undergoing VIV, and analyzed some statistical characteristics of pressure, such as mean value, variance, frequency spectrum, etc., thus the mechanism of reduction in the amplitude of VIV for a bridge deck in the presence of spanwise sinusoidal perturbation. Larsen (2012) studied the effects of size of trapezoidal box girder on the response of VIV by means of the wind tunnel test with three geometric sizes. It is demonstrated that there would be one sectional shape that had no VIV at all and the angle between bottom slab and inclined web was an important parameter. Xu (2010) investigated the mechanism of reduction in the amplitude of VIV for a streamlined box girder and found that severe fluctuation of pressure in the middle and downstream regions at the upper face constructs the fundamental momentum for vortex resonance, which are incurred due to the flow separation at the front upper face. Larsen (2000) discussed the

VIVs of the Great Belt East Bridge observed during the final phases of deck erection and surfacing of the suspended spans, and the guidevanes were designed and implemented to mitigate the VIV oscillations of Great Belt East Bridge. The vortex-induced vibrations encountered by the Storebælt suspension bridge and the Osterøy suspension bridge were mitigated efficiently by fitting guide vanes at the joints of the horizontal bottom plate and lower side panels of the box girders (Larsen and Poulin 2005). Li (2011) performed the wind tunnel testing on vortex-induced vibration of a single main cable suspension bridge and its alleviation means by altering geometric parameters of accessories of deck. The difference of section and full aeroelastic model testing results are discussed by considering the correlation of vortex-excited force along the span.

Sarwar *et al*. (2010) compared the computational flow field around the deck with and without countermeasures by CFD numerical simulation, to explain how the flow characteristics changes and how the countermeasures works. Zhou *et al.* (2006) investigated the vortex-shedding mechanism around π-shaped deck by means of discrete vortex method and flow visualization. It is concluded that the separation bubble generated at the lower windward corner and the main vortex structure developed from the separation bubble and its motion around the lower side of the prototype bridge deck are located at its lower surface and traveling across the lower side of the bridge deck downstream into the wake. The period of vortex shedding at the lower windward corner and development of vortex motion around the lower side of the prototype bridge deck make a direct influence on the value of work done by the local suction pressure induced by the vortex. Different arrange of vertical plates on π-shaped deck can convert torsional flutter to coupled flutter, thus increase the critical wind speed. Larsen (2000) used 2-D DVM software DVMFLOW to investigate the aerodynamics failure mechanism responsible for the collapse of the Tacoma Narrows Bridge. It is demonstrated that the instability mechanism is associated with the formation and drift of large vortices from the upwind edge of the bridge girder cross section. An empirical model of the vortex formation and drift process is formulated that allows critical wind speed for onset of the instability to be estimated. However, the assumption that critical wind speed is associate merely with vortex drift velocity and vortex drift velocity is constant along bridge girder section is not capable to describe the strong nonlinear phenomena of fluid-structure coupled problem.

Although VIVs of a bluff body have been widely investigated, they are not completely understood due to the complexity of the nonlinear interaction between the fluid and motion of the bluff body yet. Therefore, this paper takes the HongKong-Zhuhai-Macao Bridge as an example to study the suppression mechanism of countermeasures for VIV of a box girder with long projecting slab based on wind tunnel test and CFD. The organization of the paper is as follows: in Section2, a 1:20 large-scale section-model wind tunnel test of this bridge is conducted and the phenomenon of vertical VIV is observed during the test. In Section3, the mechanism on vortex resonance of original section is analyzed using CFD simulation, and accordingly, three types of wind fairing ---trapezoidal wind fairing, airfoil wind fairing, and smaller airfoil wind fairing--- are proposed to restrain the vertical VIV. Meanwhile, the wind velocity of upper deck surface is measured in order to investigate the variation of wind field characteristics. In Section4, wind tunnel tests in case of the sections with three different kinds of wind fairing are conducted, and finally, the conclusion is presented.

2. Background

2.1 Description of the bridge

As the main part of HongKong-Zhuhai-Macao Bridge, the non-navigable channel bridge is a 110 m-span continuous steel box-girder bridge. The stiffening girder is a single box with double chamber and double symmetrical long projecting slabs and it is 33.1m wide and 4.5m deep, as shown in Fig. 1. The width of the double slabs accounted for about 1/6 of the total width of the deck.

2.2 Test setup

A large-scale rigid sectional model of the bridge was built and tested in TJ-3 boundary layer wind tunnel at Tongji University in Shanghai, China. The wind tunnel test section is 15 m in length, 14 m in width, 2 m in height. The maximum wind velocity can be 17 m/s and the turbulence intensity of the free stream can be no stronger than 0.3%. In order to get a higher Reynolds number and meanwhile, to simulate the structure details more precisely, thus the test results can be more close to practice in this way, a rigid sectional model with a geometric scale ratio of 1:20 is designed and reproduced, as shown in Fig. 2.

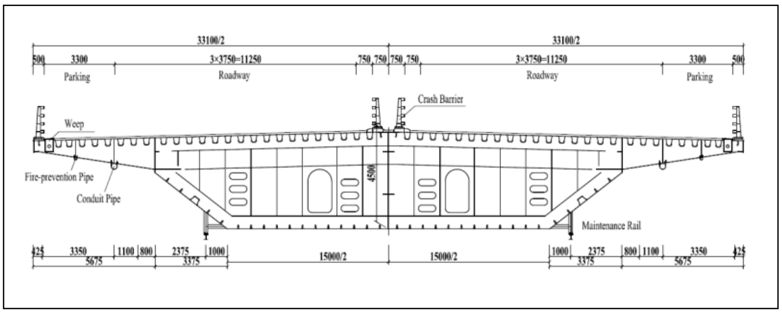

Fig. 1 Cross section of bridge deck (unit: mm)

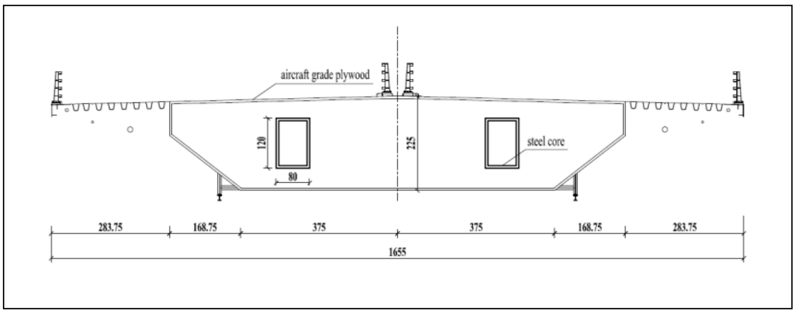

Fig. 2 Cross section of sectional model (unit:mm)

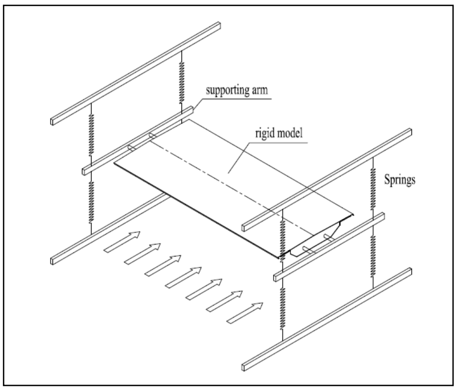

Fig. 3 Sketch of the testing device

The rigid model, 3.6 m long, 1.655 m wide, and 0.225 m deep, is made of two steel cores, connected by three similar transverse steel pipes, providing the stiffness, and a plywood skin to reproduce the aerodynamic shape. The model is supported by eight springs (see Fig. 3), allowing the vertical and torsional degrees of freedom. The stiffness and locations of the springs are chosen to reproduce the prototype ratio of the first vertical and torsional natural frequencies, and to keep the vertical and torsional vortex-shedding critical speeds within the test speed range.

According to the similarity requirements of sectional model design, as well as the frequency ratio λ_f between the real bridge and the model bridge, the wind speed ratio λ_v is determined. Thus, the relationship of the main parameters between the real bridge and the model bridge can be obtained, as shown in Table 1.

The sectional model is prepared with the length scale of $\lambda_L = L_m / L_p$ =1:20, where L_m and L_p represent the length of model and prototype, respectively. The frequency scale $\lambda_f = 1/\lambda_T = f_m / f_p$=5:1 is arbitrarily determined without considering the similarity of Froude number, which is a general practice in a sectional model test. Here λ_T is the time scale, f_m and f_p represent the frequency of the model and the prototype, respectively. The scaling of reduced velocity is satisfied as follows

$$\left(\frac{U}{fB}\right)_m = \frac{\lambda_L / \lambda_T}{\lambda_f \lambda_L}\left(\frac{U}{fB}\right)_p = \left(\frac{U}{fB}\right)_p \tag{1}$$

where U is the wind velocity and the subscripts m and p denote the model and prototype. Table 1 shows the setup parameters for the large-scale sectional model.

The damping ratio is a critical factor for evaluating VIV performance, and the VIV often decreases rapidly with increasing damping ratio of the structure. Therefore, the damping ratio of the structure during the test must be controlled well in order not to go beyond the allowable limit (0.5%). Since the damping ratio is dependent on the amplitude of the forced vibration, the consistent part of the decaying free vibration signals is utilized to identify the damping ratios before the test, as shown in Fig. 4. The damping ratio is determined as $\xi_h = \ln(h_0 / h_{30})/(2\pi\times 30)$.

- When the unimodal amplitude of the initial excitation is 7 mm, the structural damping ratio gained from the decaying free vibration curve is determined as 0.33%.
- When the unimodal amplitude of the initial excitation is 5 mm, the structural damping ratio gained from the decaying free vibration curve is determined as 0.30%.

When the unimodal amplitude of the initial excitation is 3 mm, the structural damping ratio gained from the decaying free vibration curve is determined as 0.25%.

Table 1 Similarity scales and setup parameters for sectional model wind tunnel tests

Parameters		Unit	Prototype	similarity scales	Model(target)	Model(measured)
Length	L	m	72	λ_L = 1:20	3.6	3.6
Width	B	m	33.1	λ_L = 1:20	1.655	1.655
Depth	D	m	4.5	λ_L = 1:20	0.225	0.225
Mass	m	kg/m	27000	$\lambda_m = 1:20^2$	67.5	65.4
1st Vertical Frequency	f_h	Hz	0.806	λ_f =5:1	4.03	4.101
Velocity	U	m/s	-	λ_v = 1:4	-	
Damping Ratio	ξ_h	%	0.5	1	0.5	0.3
Scruton number	Sc		0.6325		0.6325	0.3677

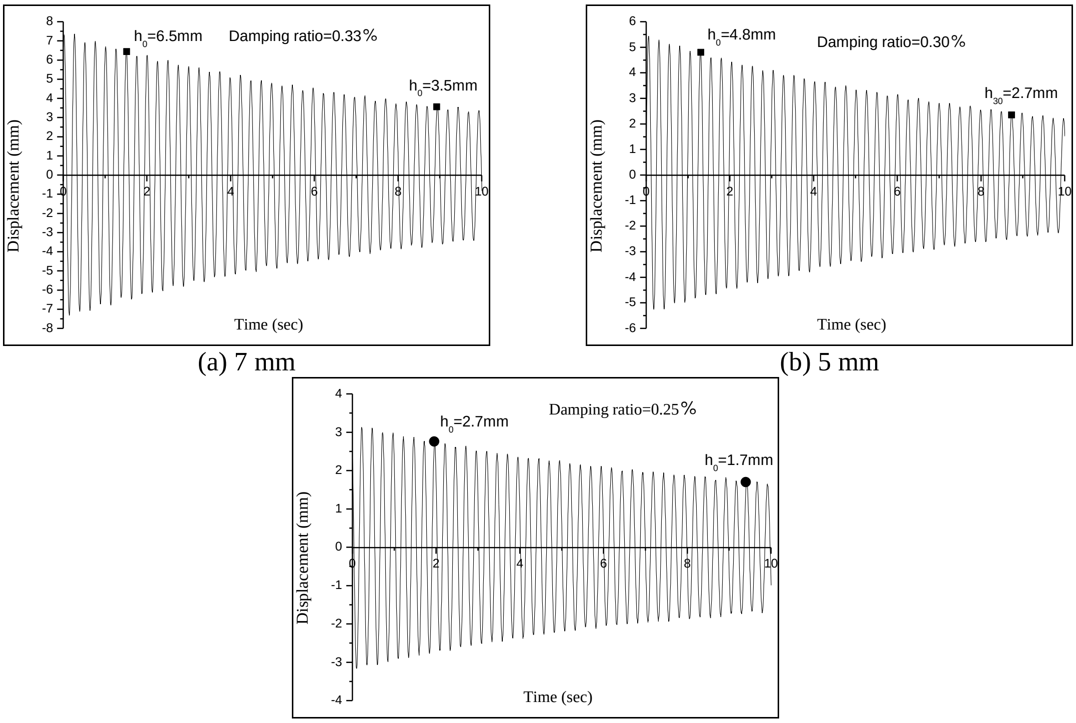

(a) 7 mm (b) 5 mm
(c) 3 mm

Fig. 4 The decaying time history used for the evaluation of damping ratio

(a) Model with crash barriers

(b) Model without crash barriers

Fig. 5 Large-scale sectional model in the wind tunnel

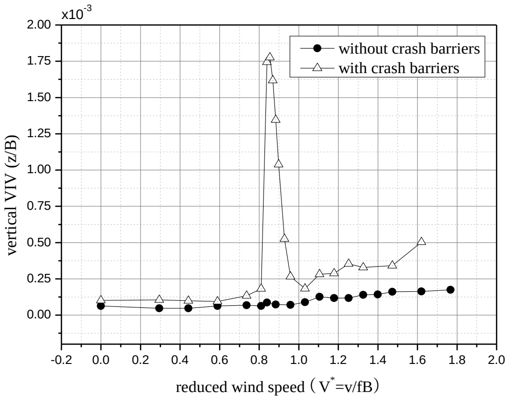

(a) $\alpha = 0°$

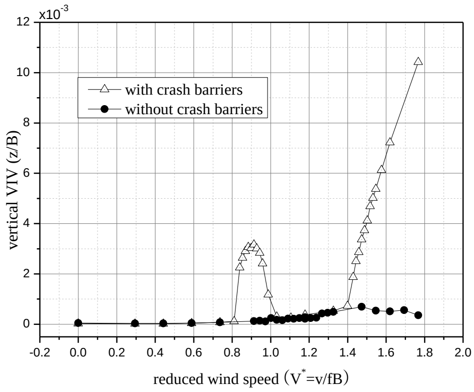

(b) $\alpha = +3°$

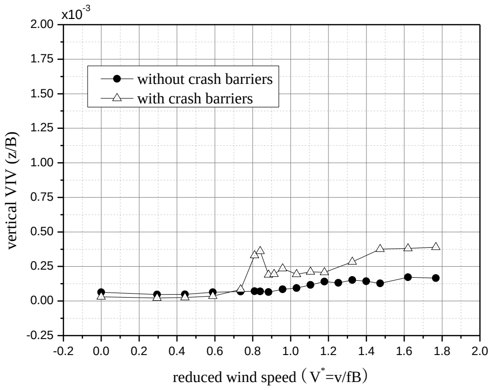

(c) $\alpha = -3°$

Fig. 6 The responses of vertical VIV

Test results

Wind tunnel tests of original section are conducted in a uniform flow and the main results are summarized as follows:

- The vertical VIV occurs in case of the original section (see Fig. 5) when $\alpha = 0°$ and $\alpha = +3°$ (α is the wind attack angle), and no noticeable vibrations were observed when $\alpha = -3°$.
- The VIV peaks at a wind velocity around 5.7-6.1 m/s when $\alpha = 0°$, with a maximum amplitude close to 3.0 mm.
- The VIV peaks at a wind velocity around 5.7-6.7 m/s when $\alpha = +3°$, with a maximum amplitude exceeding 5.0 mm. In addition, a more severe undamped vertical vibration occurs at a relatively higher range of wind speed.
- However, the vertical VIV (including the high wind speed vertical VIV) which is observed when $\alpha = 0°$ and $\alpha = +3°$ disappears when all of the crash barriers of the bridge deck section are removed under these two conditions (see Fig. 5(b)).
- A preliminary conclusion can be made from the experiment results that it is the crash barriers that cause the vertical VIV of the bridge deck.

3. Reasons and countermeasures for VIV

3.1 Cause of vortex shedding

CFD numerical simulation is employed to examine the flow characteristics around box girder section with long projecting slabs and the mechanism of reduction on oscillation amplitude in the presence of the aerodynamic countermeasures is clarified.

The numerical simulations are performed with ANSYS Fluent 6.3 based on the Finite Volume Method. The advection term is discretized using the Second-order Upwind Scheme in the spatial domain, and the transient term is discretized by the Second-order Center Scheme in the time domain. The Realizable $\kappa - \varepsilon$ model is used to calculate turbulent viscosity and the SIMPLE algorithm is used to achieve the pressure-velocity coupling. The Reynolds number is set as about 1e+6. The detailed analysis conditions of the numerical simulation are summarized in Table 2.

In the grid-based method simulation of flow around complex geometries, mesh generation takes on fundamental importance. The length and width of the computational domain are set as 55D×35D, respectively, where D is the depth of model section (see Fig. 7). A block-structured grid is used with coarser mesh in the domain area far from the section, whereas finer mesh is used for the domain area in the near solid boundary, which is 10D×3D (see Fig. 8). It not only helps to generate reasonable meshing, but also allows for use of less number of mesh with sufficient accuracy to speed up the calculation process. The total number of grids adds up to over 1e6. The size of the computational domain can be measured by the blocking probability, which reaches no more than 3% in this domain.

At the inlet boundary, a steady uniform flow velocity is given. At the outlet boundary, an opening pressure condition is applied. And for the upper and lower surfaces of the computational domain, symmetric conditions are employed.

Table 2 Analysis conditions of the CFD numerical simulation

Spatial Discretization	Advection term	Transient term	Pressure-velocity coupling	Turbulence model	Number of mesh
Finite Volume Method	Second-order Upwind differencing	Second-order Center Differencing	SIMPLE	Realizable $\kappa-\varepsilon$	Over 1e+6

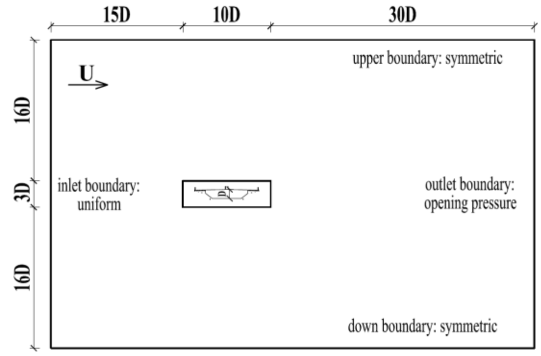

Fig. 7 Overview of computational domain and boundary conditions

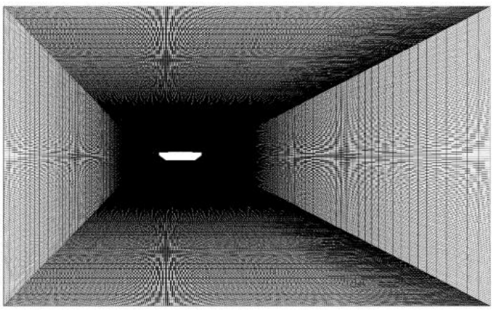

Fig. 8 Mesh of the computational domain

The forming of VIV cannot get away from the periodic vortex-shedding around the box girder. Figs. 9 and 10 show the cloud image of velocity field around the original section when $\alpha=0°$ and $\alpha=+3°$. From the two figures, the vortex-shedding characteristics can be clearly investigated.

The results in Fig. 9 show that the distributions of the velocity field around the upper surface of deck behind the crash barrier are non-uniform, indicating that vortices are largely concentrated in this region. Though another vortex-shedding behind the maintenance rail can be also observed, it is too far away from the main deck. There is no denying that the oscillating force acting on the box girder by vortex-shedding will increase with the increase of vortice strength, but will decrease with the increase of the distance between the vortex core and the main deck. Based on this knowledge, this alternate vortex-shedding has little influence on the behavior of the box girder.

According to Fig. 9, an obvious phenomenon of separated vortex-shedding, which can be called v_1 in this paper, can be observed around the upper surface of the curb. Independently, the separated vortices v_2 can be seen to form around the upper surface of deck behind the crash barrier, which is larger and more considerable than the previous one. All in all, the phenomenon of periodic vortex-shedding exists in the region of both the surface of the curb and the deck.

From Fig. 10, the separated vortices v_2 can be seen to generate behind the bottom rail, because the distance between the curb and crash barrier is not long enough to accelerate the flow velocity between them, resulting in an approximately stagnation region forming behind the crash barrier and curb. Even though the end part of the curb is changed into chamfer, the separated vortices v_2 still exists.

Based on the understanding mentioned above, the forming of VIV of the box girder owes to the phenomenon of the periodic vortex-shedding around the deck upper surface, including the separated vortices v_1 and v_2, in particular the separated vortices v_2.

The Scruton number is a critical factor for evaluating VIV performance, and the VIV often decreases rapidly with increasing Scruton number of the structure. On the other hand, the deck to reach very large vibration amplitudes in case of low Scruton numbers.

$$Sc = 2\pi \frac{m\xi_h}{\rho B^2} \tag{2}$$

where m is the mass per unit length, ξ_h is the structural damping ratio, B is the deck chord and ρ is the air density.

In order to better understand the relationship between the amplitude of VIV and Scruton number, the CFD numerical simulation were carried out for three damping ratios (ξ_h=0.001, ξ_h=0.003, ξ_h=0.006) at $\alpha = 0°$. Fig. 11 presents the non-dimensional oscillation amplitude, flexural motion as function of the reduced velocity varying the Scrouton number.

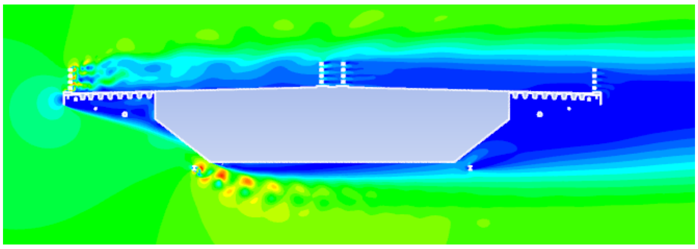

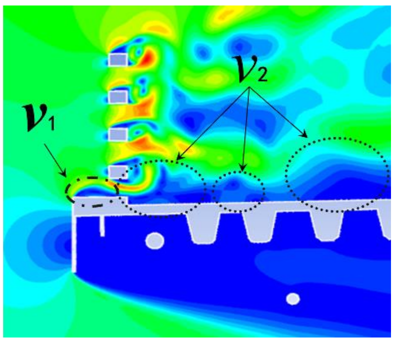

Fig. 9 Cloud image of velocity when $\alpha = 0°$

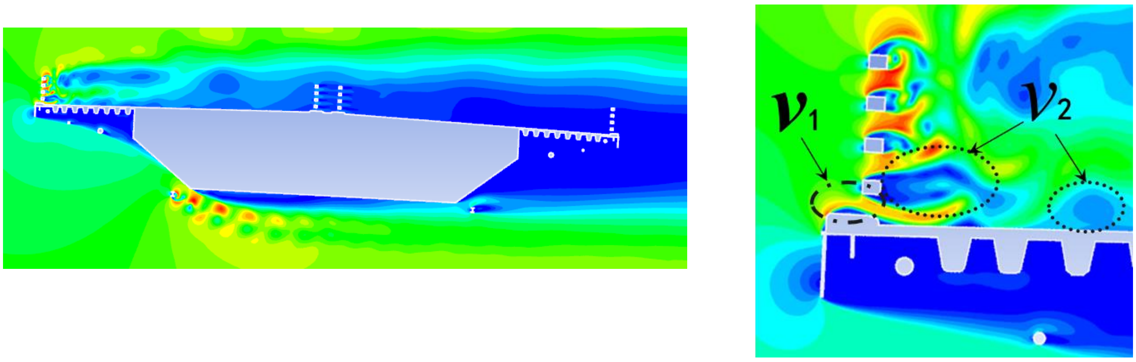

Fig. 10 Cloud image of velocity when $\alpha = +3°$

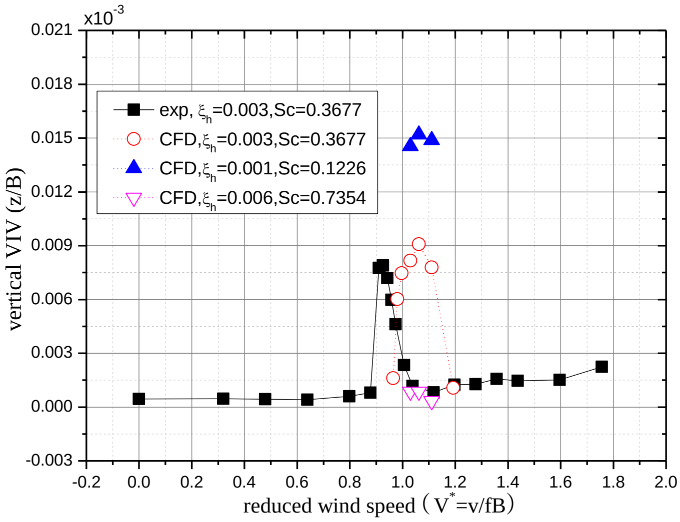

Fig. 11 Steady state response: nondimensional oscillation amplitude, flexural motion as function of the reduced velocity varying the Scrouton number (ξ_h =0.001; ξ_h =0.003; ξ_h =0.006)

3.2 Countermeasures to suppress VIV

The above analysis indicates that the stagnation region forming between the side crash barrier and curb gives rise to the separated vortices v_2, which is the main cause of the VIV in this paper. Therefore, if the flow velocity in this region is increased, the VIV of the box girder may be suppressed. Based on this knowledge, three Schemes are proposed to control the VIV and the control effectiveness is investigated through the CFD numerical simulation. The schemes are presented as follows: Scheme 1, a kind of trapezoidal wind fairing is installed on the side of curb, as shown in Table 3(a); Scheme 2, a kind of airfoil wind fairing is installed on the side of curb, as shown in Table 3(b); Scheme 3, a kind of smaller wind fairing is installed on the side of curb, as shown in Table 3(c).

Table 3 Three proposed schemes

Schemes	Schematic Diagram	Model in the test
(a) trapezoidal wind fairing	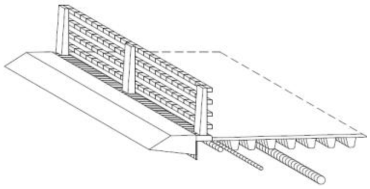	
(b) airfoil wind fairing	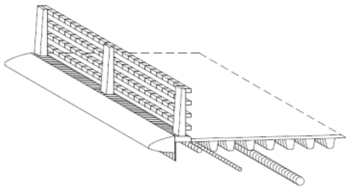	
(c) smaller airfoil wind fairing	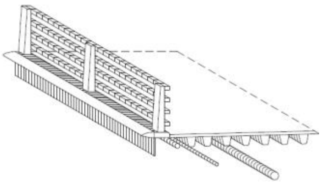	

Changes in the characteristics of the time-averaged velocity field are pursued to understand the mechanism of reduction in amplitude of vibration by such countermeasures. Fig. 12 shows the comparisons of the CFD numerical simulations between the original section and the sections with three schemes. The main conclusions can be summarized as follows:

- The average velocity of the field near the deck under the original section is quite low.
- The flow velocity between the crash barrier and the curb can be increased at a different degree under the sections with Scheme 1, 2 and 3.
- The increasing of the flow velocity between the crash barrier and the curb result in the reduction of the strength of the separated vortices v_2, thus suppressing the VIV of the bridge finally.

3.3 Analysis of velocity testing results

Wind velocity of upper deck surface is measured using 3-dimensional wind speed instrument. The Cobra Probe is a dynamic multi-hole pressure probe for measuring mean and fluctuating 3-component velocities and static pressure. Original section and section with airfoil wind fairing are tested under the wind velocity of maximum VIV amplitude. Measuring points (see Fig. 13) are located 80~560 mm behind the crash barriers with height of 32 mm, 65 mm, 120 mm from the surface of the deck, respectively.

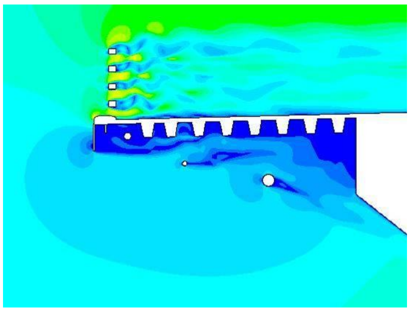

(a) original section

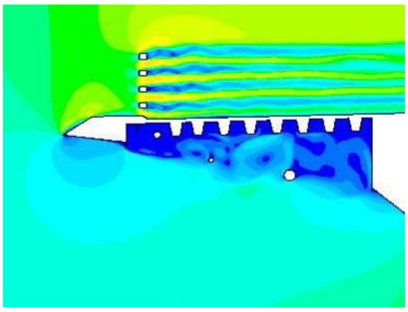

(b) with trapezoidal wind fairing

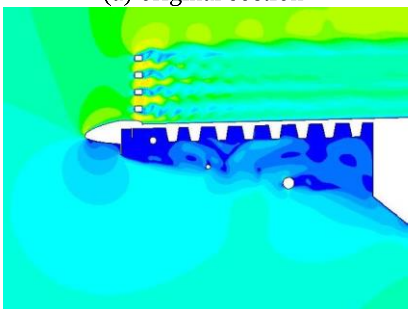

(c) with airfoil wind fairing

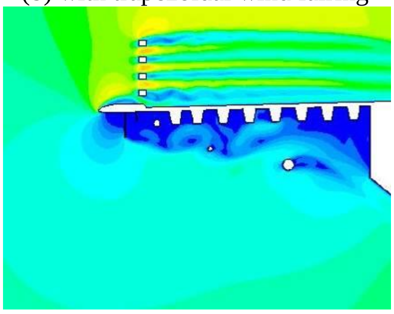

(d) with smaller airfoil wind fairing

Fig. 12 Velocity field of original section and sections with countermeasures

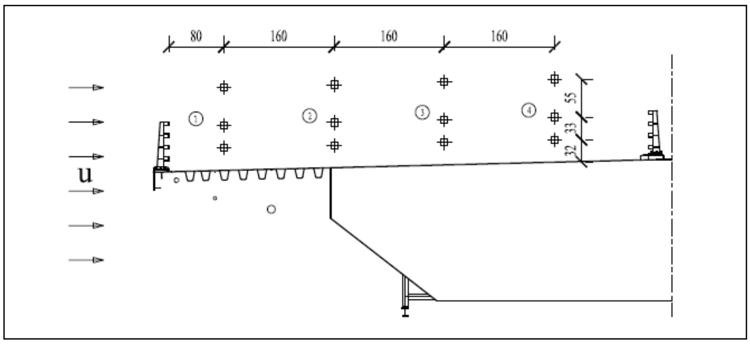

Fig. 13 Locations of the Cobra Probe measuring points

The mean value and power spectrum density (PSD) of wind velocity of each measuring point of original section and section with airfoil wind fairing under the wind velocity of maximum VIV amplitude are shown in Figs. 14 and 15. Wind velocity of section with airfoil wind fairing have a larger value than that of original section, which means that airfoil wind fairing contributes to speeding up of the wind velocity field behind the crash barrier. Vibration energy of original section is mostly concentrated at the natural frequency and the vibration energy is reduced noticeably with the help of airfoil wind fairing.

Considering that wind pressure in the neighborhood of the bridge deck has much more effect on the box girder than the pressure far away, the wind speed PSD of the bottom measuring points are listed in Fig. 16. Wind speed energy of low frequencies (0-100 Hz) is reduced obviously under the section with airfoil wind fairing at all four positions, and those small wind energy at low frequency are not big enough to cause VIV.

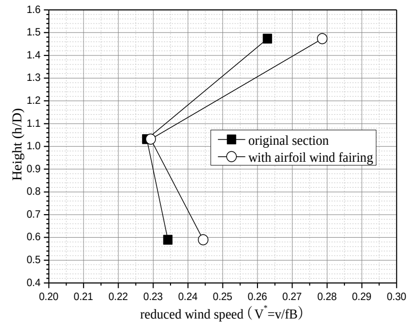

(a) Average wind speed at position 1

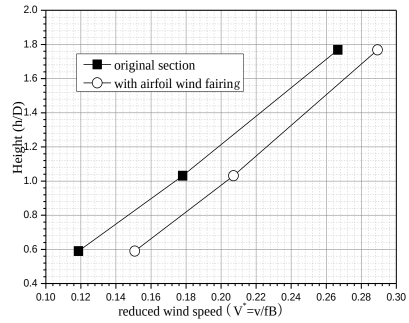

(b) Average wind speed at position 2

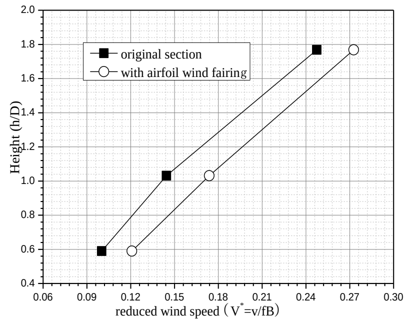

(c) Average wind speed at position 3

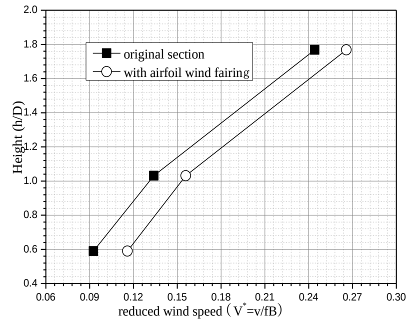

(d) Average wind speed at position 4

Fig. 14 Average wind speed at four positions under the maximum VIV amplitude

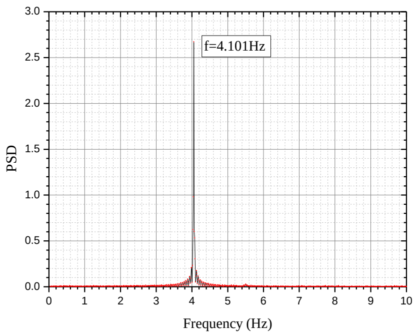

(a) original section

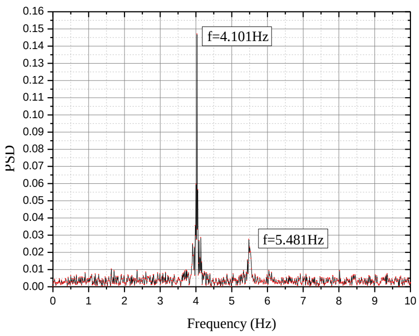

(b) with airfoil wind fairing

Fig. 15 wind speed PSD of two sections under the maximum VIV amplitude

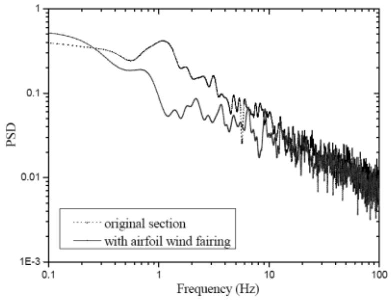

(a) Bottom point of Position 1

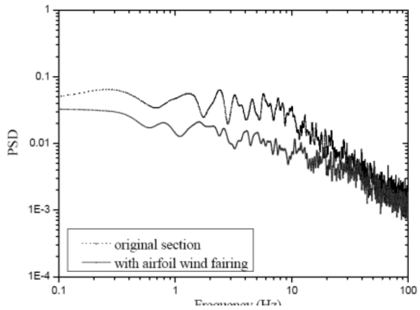

(b) Bottom point of Position 2

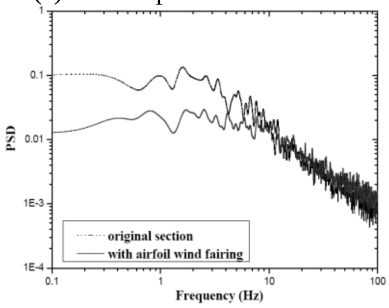

(c) Bottom point of Position 3

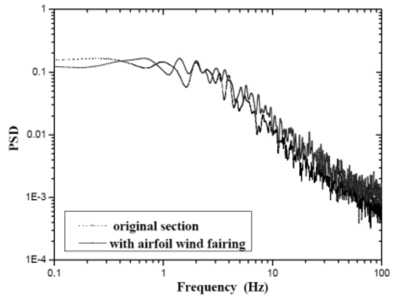

(d) Bottom point of Position 4

Fig. 16 Wind Speed PSD at the bottom point of four positions (in double logarithm coordinates)

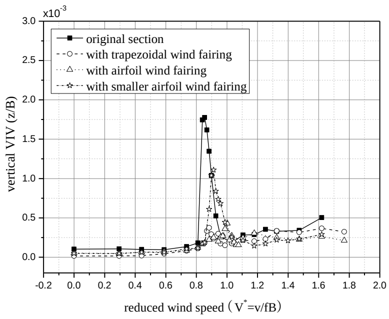

(a) $\alpha = 0°$

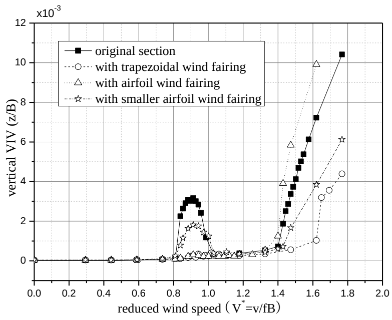

(b) $\alpha = +3°$

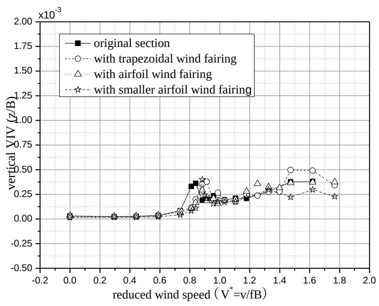

(c) $\alpha = -3°$

Fig. 17 Test results of original section and sections with countermeasures

4. Experiment results of deck with countermeasures

Wind tunnel tests in case of the sections with three different countermeasures mentioned above have been conducted and the results compared with the original section are shown in Fig. 17.

- All the three different countermeasures can be used to control VIV to varying degrees.
- When $\alpha = 0°$, for scheme 1 and 2, the oscillation amplitudes of the box girder are close to zero, so the VIV is completely suppressed.
- When $\alpha = 0°$, for scheme 3, the maximum vertical VIV amplitude is greatly reduced, reaching approximately half the value of the original section (2 mm);
- When $\alpha = +3°$, the results are almost similar to that under the condition of $\alpha = 0°$.
- When $\alpha = -3°$, there are no special phenomenon when using three schemes.

5. Conclusions

In this paper, research based on large-scale section-model wind tunnel test and CFD numerical simulation on the suppression mechanism and aerodynamic countermeasures for VIV of a box girder with long projecting slab has been done. The main conclusions can be drawn as follows:

- The results of wind tunnel test show that it is the crash barrier that induces the Vertical VIV. CFD numerical simulation results show that the distance between the curb and crash barrier is not long enough to accelerate the flow velocity between them, resulting in an approximate stagnation region forming behind those two, where the continuous vortex-shedding occurs , giving rise to the vertical VIV in the end.
- According to the above, three types of wind fairing (trapezoidal, airfoil and smaller airfoil) are proposed to accelerate the flow velocity between the crash barrier and curb in order to avoid the continuous vortex-shedding. Both of the CFD numerical simulation and the velocity field measurement show that the flow velocity of all the measuring points in case of the section with airfoil wind fairing, can be increased greatly compared to the results of original section, and the energy is reduced considerably at the natural frequency, indicating that the wind fairing do accelerate the flow velocity behind the crash barrier.
- Wind tunnel tests in case of the sections with three different countermeasures mentioned above are conducted and the results compared with the original section show that all the three different countermeasures can be used to control VIV to varying degrees.

Acknowledgments

The authors gratefully acknowledge the support of National Key Basic Research Program of China (i.e.973 Program) (2013CB036300).

References

Bearman, P.W. (1984), "Vortex shedding from oscillating bluff bodies", *Annu. Rev. Fluid Mech*., **16**, 195-222.

Chen, A.R. and Zhou, Z.Y. (2006), "On the mechanism of vertical stabilizer plates for improving aerodynamic stability of bridges", *Wind Struct.*, **9**(1), 59-74.

Diana, G., Resta, F., Belloli, M. and Rocchi, D. (2006), "On the vortex shedding forcing on suspension bridgedeck", *J. Wind Eng. Ind. Aerod*., **94**(5), 341-363.

Diana, G., Rocchi,D., Argentini, T. and Muggiasca, S. (2010), "Aerodynamic instability of a bridge deck section model:linear and nonlinear approach to force modeling", *J. Wind Eng. Ind. Aerod*., **98**(6-7), 63-374.

Diana, G., Resta, F. and Rocchi, D. (2008), "A new numerical approach to reproduce bridge aerodynamic non-linearities in time domain", *J. Wind Eng. Ind. Aerod*., **96**(10-11), 1871-1884.

Diana, G., Fiammenghi, G., Belloli, M. and Rocchi, D. (2013), "Wind Tunnel tests and numerical approach for long span bridges: the Messina bridge" , *J. Wind Eng. Ind. Aerod*., **122**, 38-49.

El-Gammal, M., Hangan, H. and King, P. (2007), "Control of vortex shedding-induced effects in a sectional bridge model by spanwise perturbation method", *J. Wind Eng. Ind. Aerod*., **95**(8), 663-678.

Gabbai, R.D. and Benaroya, H. (2005), "An overview of modeling and experiments of vortex-induced vibration of circular cylinders", *J. Sound Vib*., **282(**3-5), 575-616.

Larsen, A. (2000), "Aerodynamics of the Tacoma Narrow Bridge: 60 Years Later", *J. Struct. Eng. Int.*, **10**(4), 243-248.

Larsen, A., Esdahl, S., Andersen, J.E. and Vejrum, T. (2000), "Storebæl suspension bridge—vortex shedding excitation and mitigation by guide vanes", *J. Wind Eng. Ind. Aerod.*, **88**(2-3), 283-296.

Larsen, A. and Poulin, S. (2005), "Vortex shedding excitation of box-girder bridges and mitigation", *J. Struct. Eng. Int*., **15**(14), 258-263.

Larsen, A. and Wall, A. (2012), "Shaping of bridge box girders to avoid vortex shedding response", *J. Wind Eng. Ind. Aerod*., **104-106**, 159-165.

Li, M.S., Sun, Y.G., Liao, H.L. and Ma, C.M. (2011), "Wind tunnel investigation on vortex-induced vibration for a suspension bridge by section and full aeroelastic modeling", *Proceedings of the 13th International Conference on Wind Engineering*, July 10-15, Amsterdam.

Li, H., Ma, S.J., Zhang, Q.Q., Li, N. and Liu, Z.Q. (2014), "Field monitoring and validation of vortex-induced vibrations of a long-span suspension bridge", *J. Wind Eng. Ind. Aerod*., **124**, 54-67.

Marra, A.M., Mannini, C. and Bartoli, G. (2011), "Van der Pol-type equation for modeling vortex-induced oscillations of bridge decks", *J. Wind Eng. Ind. Aerod*., **99**(6-7), 776-785.

Nagao, F., Utsunomiya, H., Yoshioka, E. and Ikeuchi, A. (1997), "Effects of handrails on separated shear flow and vortex-induced oscillation", *J. Wind Eng. Ind. Aerod*., **69-71**, 819-827.

Prasanth, T.K. and Mittal, S. (2008), "Vortex-induced vibrations of a circular cylinder at low Reynolds numbers", *J. Fluid. Mech.*, **594**, 463-491.

Ricciardelli, F., de Grenet, E.T. and Hangan, H. (2002), "Pressure distribution, aerodynamic forces and dynamic response of box bridge sections", *J. Wind Eng. Ind. Aerod*., **90**(10), 1135-1150.

Sanchez-Sanz, M. and Velazquez, A. (2009), "Vortex-induced vivration of a prism in internal flow", *J. Fluid. Mech.*, **641**, 431-440.

Sarwar, M.W. and Ishihara, T. (2010), "Numerical study on suppression of vortex-induced vibrations of box girder bridge section by aerodynamic countermeasures", *J. Wind Eng. Ind. Aerod*., **98**(12), 701-711.

Sarpkaya, T. (2004), "Acritical review of the intrinsic nature of vortex-induced vibrations", *J. Fluid. Struct*., **19**(4), 389-447.

Wu , T. and Kareem, A. (2013), "Vortex-induced vibration of bridge decks: volterra series-based model", *J. Eng. Mech. - ASCE,* **139**(12), 1831-1843.

Wang, Z.J. and Zhou, Y. (2005), "Vortex-induced vibration characteristics of an elastic squre cylinder on fixed supports", *J. Fluid. Eng. -T ASME*, **127**(2), 241-249.

Williamson, C.H.K. and Govardhan, R. (2004), “Vortex-inducedvibrations”, *Annu. Rev. Fluid Mech.*, **36**, 413-455.
Xu, F.Y., Lin, Z.X., Li, Y.N. and Lou, W.J. (2010), “Vortex resonance depression mechanism of a bridge deck with aerodynamic measures”, *J. Vib. Shock*, **29**(1), (in Chinese).

CC